# TRANSPORT PROPERTIES AND TRANSPORT PHENOMENA IN CASTING NICKEL SUPERALLOYS[1]

S. D. Felicelli,[2] P. K. Sung,[3] D. R. Poirier,[3] and J. C. Heinrich[2,4]

---

[1]Paper presented at the Thirteenth Symposium on Thermophysical Properties, June 22-27, 1997, Boulder, Colorado, U.S.A.

[2]Department of Aerospace and Mechanical Engineering, The University of Arizona, Tucson, Arizona 85721, U.S.A.

[3]Department of Materials Science and Engineering, The University of Arizona, Tucson, Arizona 85721, U.S.A.

[4]Author to whom correspondence should be addressed.

**ABSTRACT**

Nickel superalloys that are used in the high-temperature regions of gas-turbine engines are cast by directional solidification (DS). In DS processes, the castings are cooled from below, and three zones exist during solidification: (1) an all-solid zone at the bottom, (2) a "mushy zone" that is comprised of solid and liquid material, and (3) an overlying all-liquid zone. Computer simulations can be useful in predicting the complex transport phenomena that occur during solidification, but realistic simulations require accurate values of the transport properties. In addition to transport properties, the thermodynamic equilibria between the solid and liquid during solidification must also be known with reasonable accuracy. The importance of using reasonably accurate estimations of the transport properties is illustrated by two-dimensional simulations of the convection during solidification and the coincidental macrosegregation in the DS castings of multicomponent Ni-base alloys. In these simulations, we examine the sensitivity of the calculated results to measured partition ratios, thermal expansion coefficients, and viscosities that are estimated by regression analyses and correlations of existing property data.

**KEY WORDS:** directional solidification; freckles, multicomponent alloys; nickel superalloys.

## 1. INTRODUCTION

In the directional solidification (DS) process, solidification is effected vertically by cooling from below. The process provides an effective means of controlling the grain shape, producing a columnar microstructure with all of the grain boundaries parallel to the longitudinal direction of the casting. In conjunction with a grain selector or a preoriented seed at the bottom of the casting, directional solidification is used to make entire castings that are dendritic single crystals (SC) [1].

Unfortunately, segregation defects known as freckles can be found in DS and SC castings; they are cause to scrap these expensive castings. These segregates are observed as long and narrow trails, aligned roughly parallel to the direction of gravity in DS castings, and are enriched in the normally segregating elements and depleted of the inversely segregating elements. It is known that freckles are a direct consequence of upward flowing liquid plumes that emanate from channels within the mushy zone (e.g., see Hellawell *et al*. [2]). In terms of transport phenomena, the channels are a manifestation of thermosolutal convection in a porous media subject to remelting by interdendritic liquid laden with solute.

Because of the technological importance of DS and SC castings of superalloys, many studies have been made on simulating transport phenomena in directionally solidified castings with the full set of conservation equations. In 1991, Felicelli *et al*. [3] simulated channels and freckles in directional solidified Pb-Sn alloys. Related numerical works since 1991 include Poirier and Heinrich [4] and Neilson and Incropera [5].

When cooling a binary alloy from below (as in DS and SC processes), the temperature profile is gravitationally stable, but strong convection may develop especially when solute that is lighter than

the solvent is rejected to the liquid. In a multicomponent alloy, however, each alloying element contributes its change to the density. Some components decrease the liquid density, while others increase it, depending on their respective solutal expansion coefficients.

The prediction of macrosegregation in alloys with two or more solutes dates back to 1970, when Fujii *et al.* [6] considered a simplified model of convection in the mushy zone only. Models for multicomponent alloys that include thermosolutal convection, both in the liquid and mushy zone, started appearing in 1995 [7-9] and will probably be widely applied in the near future due to the fact that most alloys of practical interest comprise many elements. The modeling of multicomponent alloys requires different algorithmic strategies than the one used for binary alloys. In particular, knowledge of the temperature in the mushy zone does not automatically provide the concentration in the interdendritic liquid. In a multicomponent alloy, many combinations of the liquid concentrations can have the same liquidus temperature, making it more difficult to calculate the solidification path.

In order to model the transport phenomena and macrosegregation during dendritic solidification of alloys, the density of the liquid must be known. The temperature and the concentrations of the elements in the interdendritic liquid vary, so a method has been devised to estimate its density. Since the simulation of the solidification on Ni-base superalloys is of particular interest, the density of many of the liquid transition-metals and aluminum and the change in density with temperature, called the temperature coefficient of liquid density ($d\rho/dT$, where $\rho$ is density and $T$ is temperature), were gathered, reviewed, and reduced in a simple correlation [10]. The correlation was used to critically evaluate the temperature coefficients, which are not well established for many

of the transition-metals with high melting points. It also can be used to estimate $d\rho/dT$ of the transition-metals for which there are no reported data. Also, this procedure was applied to estimate the liquid densities of five Ni-base superalloys as a verification [10].

In this article, the directional solidifications of a Ni-Al-Ta-W alloy and of a Ni-Al-Ta alloy. are modeled. In both alloys, aluminum partitions to the interdendritic liquid in the mushy zone. Hence its concentration increases with distance below the leading part of the mushy zone, making the liquid less dense from below. This, of course, tends to make the liquid convectively unstable. Tantalum also partitions to the interdendritic liquid, but it makes the liquid more dense from below. Hence, it tends to make the liquid stable with respect to convection. Tungsten, like tantalum, increases the density of the interdendritic liquid, but it partitions to the solid so that it tends to make the liquid unstable with respect to convection. Hence, both aluminum and tungsten are solutes that enhance convection and make the alloy more prone to the formation of freckles. Since aluminum partitions weakly and tungsten partitions strongly, however, the simulations show that tungsten is the more serious culprit in forming freckles.

The buoyancy of the interdendritic liquid can be found in the body-force term of the momentum equation, which is given in the next section. As is often done, the density of the liquid in the body-force term is expressed as

$$\rho = \rho_0 \left[ 1 + \beta_T (T - T_R) + \sum_{j=1}^{N} \beta_c^j (c_l^j - c_R^j) \right] \tag{1}$$

where ρ is the density of the liquid; $T$ is temperature; $c_l^j$ is the concentration of solute $j$ in the liquid; $N$ is the number of solutes in the alloy; and $\rho_0$ is the density of the alloy at the reference temperature, $T_R$, and the reference composition of the alloy, $c_R^1$, $c_R^2$, ...., $c_R^N$. The coefficients $\beta_T$ and $\beta_c^j$'s are the thermal expansion coefficient and the solutal expansion coefficients, respectively. They are defined as

$$\beta_T = \frac{1}{\rho_o} \frac{\partial \rho}{\partial T} \tag{2}$$

$$\beta_c^j = \frac{1}{\rho_o} \frac{\partial \rho}{\partial c_l^j} \tag{3}$$

The effects of varying three important properties on thermosolutal convection and macrosegregation patterns in a Ni-Al-Ti-W alloys are examined in the following simulations. The partitioning of each element between the solid and the liquid is quantified by its equilibrium partition ratio, defined as

$$k^j = \frac{\bar{c}_s^j}{c_l^j} \tag{4}$$

Here $\bar{c}_s^j$ is the concentration of solute $j$ of the solid at the local solid-liquid interface. Since tungsten is the major contributor effecting the thermosolutal convection, a simulation of a base-case alloy (using what we believe to be the best value of $k^W$) is carried out and repeated with $k^W$ varied by ±10%. The results of additional simulations with $\beta_c^W$ varied by ±20% and the viscosity, $\mu$, varied by ±25% are also presented. In the final simulations, tungsten is omitted from the alloy chosen as the base-case.

## 2. SOLIDIFICATION MODEL

The model for solidification of multicomponent alloys is an extension of a model for binary alloys developed by Felicelli *et al.* [3]. It is based on the following simplifying assumptions:

1. Only solid and liquid phases are present. No pores form.
2. The liquid is Newtonian and incompressible, and the flow is laminar and two dimensional.
3. The solid and liquid phases have equal and constant physical properties.
4. There is no diffusion in the solid phase.
5. The solid phase is stationary, and the fluid satisfies the Boussinesq approximation.

With these assumptions, the equations governing the fluid flow and heat and mass transport are:

Continuity:

$$\nabla \cdot \mathbf{u} = 0 \tag{5}$$

Momentum:

$$\phi \frac{\partial}{\partial t}\left(\frac{\mathbf{u}}{\phi}\right) + \frac{\mu}{\rho_0}\phi\,\mathbf{K}^{-1}\mathbf{u} - \frac{\mu}{\rho_0}\nabla^2\mathbf{u} + \frac{\phi}{\rho_0}\nabla p = -\frac{1}{\phi}\mathbf{u}\cdot\nabla\left(\frac{\mathbf{u}}{\phi}\right) + \frac{\rho\phi}{\rho_0}\mathbf{g} \tag{6}$$

Energy:

$$\frac{\partial T}{\partial t} - \alpha\nabla^2 T = -\frac{L}{c}\frac{\partial\phi}{\partial t} - \mathbf{u}\cdot\nabla T \tag{7}$$

Conservation of Solute Components:

$$\frac{\partial \bar{c}^j}{\partial t} = \nabla \cdot D^j\phi\nabla c_l^j - \mathbf{u}\cdot\nabla c_l^j \qquad j = 1, \ldots, N \tag{8}$$

In these equations, $\nabla$ is the gradient operator, **u** is the velocity, $\phi$ is the volume fraction of liquid, $t$ is time, $\mu$ is the viscosity, **K** is the permeability, $p$ is the pressure, **g** is the gravity, $\alpha$ is the thermal diffusivity, $L$ is the latent heat, $c$ is the specific heat, and $D^j$ is the diffusion coefficient of alloy $j$ in the liquid phase. The thermodynamic and transport properties used in the calculations are given in Table 1. The permeability is expressed in the principal directions in terms of the volume fraction of liquid, $\phi$, and the primary dendrite arm spacing, $d_1$.

The total concentrations of the alloy components in the mixture, $\bar{c}^j$, and the concentration in the liquid and solid phases are related by

$$\bar{c}^j = \phi c_l^j + (1 - \phi) c_s^j \tag{9}$$

and, because no diffusion in the solid is assumed, $c_s^j$ is given by

$$c_s^j = \frac{1}{1 - \phi} \int_{\phi}^{1} k^j c_l^j \, \mathrm{d}\phi \tag{10}$$

Finally, the model assumes that the liquidus temperature of the alloy in the mushy zone is a function of its local composition (no undercooling is allowed) and is expressed as

$$T_L = \mathrm{F}(c_l^j) \tag{11}$$

The particular form of the function F used in this work is given in Table 1. The equations discussed above have been discretized and integrated in time using a finite element algorithm that has already been described by Felicelli *et al.* [9, 11] and will not be repeated here.

## 3. RESULTS AND DISCUSSION

A quaternary Ni-base alloy was directionally solidified by simulation in a rectangular mold of dimensions 10 mm in the horizontal direction and 20 mm in the vertical direction. The composition of the alloy was 6 wt. pct. Al, 6 wt. pct. Ta, 5 wt. pct. W, and the balance Ni.

The simulations start with an all-liquid alloy of the nominal composition in a stable initial vertical temperature gradient such that the bottom temperature is slightly above that of the alloy melting temperature, $T_R$. Starting at time $t = 0$, a constant cooling rate, $r$, is applied at the bottom of the mold, and a constant temperature gradient, $G$, is imposed at the top. Also at $t = 0$, a small random perturbation is introduced in the solute concentration fields in order to excite the convection. The full set of boundary and initial conditions is shown in Figure 1. The applied cooling rate at the bottom of the mold was $r = 0.044$ K/s, and the temperature gradient was $G = 2000$ K/m. With these cooling conditions, the solidification proceeded with a growth rate of approximately 0.015 mm/s.

A benchmark case was first calculated using the best available estimates of the physical properties (Table 1). Then, six more cases were calculated in which the partition ratio of W ($k^{\mathrm{W}}$), the solutal expansion coefficient of W ($\beta_c^{\mathrm{W}}$), and the melt viscosity ($\mu$) were increased and decreased by a certain percentage of the reference values. The description of the cases calculated is as follows, where the variations (with corresponding signs) are with respect to the reference values:

| Case | Variation |
|---|---|
| 0 | benchmark |
| 1 | $k^{\mathrm{W}} = -10\%$ |
| 2 | $k^{\mathrm{W}} = +10\%$ |
| 3 | $\beta_c^{\mathrm{W}} = -20\%$ |

4 $\beta_c^W = +20\%$

5 $\mu = -25\%$

6 $\mu = +25\%$

All cases were simulated up to 15 min. of solidification, and the resulting macrosegregation of W was compared in order to observe the effect of uncertainties in the properties on the calculated macrosegregation patterns.

The results are shown in Figures 2a-g; shaded contours of the mixture concentration of W are plotted using the same gray scale in all figures. Figure 2a is the benchmark case. The approximate limits of the mushy zone are between 4 mm and 14 mm. Above 14 mm, the alloy is all liquid and below 4 mm it is mostly solidified. It is observed that the selected cooling rate and temperature gradient produced a freckling situation, in which channels with depleted concentration of W form along the vertical surface. The maximum depletion is 4.43 wt. pct., about 11% less than the initial concentration of W. A few spots with negative segregation are also observed in the interior of the alloy, and a region of positive segregation is found next to regions of negative segregation in all cases. The maximum positive segregation is 5.69 wt. pct., about 11% more than the initial concentration of W. This value does not include the thin solute-rich layer that formed along bottom of the mold.

Figures 2b and 2c show the segregation of W for cases 1 and 2, respectively. It is seen that a 10% increase in the value of the partition ratio causes stronger channels on the vertical surface, as well as more segregation activity in the interior of the mold (Fig. 2c). The minimum and maximum values of concentration differ as much as 21% from the initial values. On the other hand, the interior

is relatively homogeneous and the segregation on the walls is weaker when the partition ratio is decreased by 10% (Fig. 2b).

The simulations for cases 3 through 6 show effects similar to those found when the partition ratio of W is varied. When $\beta_c^{\mathrm{W}}$ is increased by 20% (Fig. 2e) or when $\mu$ is decreased by 25% (Fig. 2f), the interior of the alloy shows more segregation activity; when $\beta_c^{\mathrm{W}}$ and $\mu$ are changed in the opposite directions, the interior is more homogeneous (Figs. 2d and 2g). However, the absolute values of segregation are very similar to those of the benchmark case, in spite of the larger percentage changes in $\beta_c^{\mathrm{W}}$ and $\mu$. This differs from the higher sensitivity of the segregation strength to variations in $k^{\mathrm{W}}$.

A simulation for an alloy without W, namely Ni-6% Al-6% Ta (wt. pct.), using the same cooling conditions as for the quaternary alloy is also included. The results (Figure 3) indicate a practically stable situation, with no channels and hardly any segregation, confirming the fact that W is the element responsible for the introduction of convective instabilities and freckle formation.

A second set of calculations on the benchmark case, increasing the cooling rate, $r$, while keeping the temperature gradient at 2000 K/m, shows channels up to $r$ = 0.10 K/s. At $r$ = 0.12 K/s, the system is stable and there is no convection or channels. Keeping $r$ = 0.12 K/s, cases 2, 4, and 5, which drive the system to a more convection-prone state, were repeated. All three cases are unstable and exhibit the same freckling pattern observed at $r$ = 0.10 K/s, which consisted of one internal channel. Figure 4a shows the mixture concentration of W at $t$ = 8 min for $r$ = 0.12 K/s and with $k^{\mathrm{W}}$ increased by 10% from the reference value. In Figure 4b, the corresponding contour lines of fractions of liquid and velocity vectors show the typical patterns observed during channel formation. The

switching from no channels to channels at $r$ = 0.12 K/s still occurred when we varied $k^{W}$ by +5%, $\beta_c^{W}$ by +10%, or $\mu$ by -10%.

## 4. CONCLUSIONS

A finite element model of the solidification of dendritic multicomponent alloys has been constructed to study macrosegregation resulting from the convection that develops in the directional solidification process. The two-dimensional model has allowed us to study in detail the mechanisms that produce convection and the effect of convection on macrosegregation. In particular, we have been able to determine that freckles are a direct consequence of flow instabilities in the mushy zone. Given the sensitivity of the resulting convection to changes in some of the physical properties, we have demonstrated the need for a comprehensive data base in the future as models of this type are used in the design of casting processes. Specifically, these results show that inaccuracies in the measured physical properties can lead to the wrong prediction as to whether an alloy, solidified under conditions that are borderline between freckling or no freckling, show the undesired defects. In particular, the development of "maps" in parameter spaces to show when freckles can be expected to occur depend on the availability of accurate physical properties for the alloys.

## ACKNOWLEDGMENTS

This work was supported by the Advanced Projects Research Agency under the Micromodeling Program of the Investment Casting Cooperative Arrangement, contract MDA972-93-2-0001. The

provision of financial support for Dr. S. Felicelli by the Consejo Nacional de Investigaciones Científicas y Tecnicas (CONICET, Argentina) and the Argentina Atomic Energy Commission is gratefully acknowledged.

**REFERENCES**


1. P.R. Beeley, "Application to Aerospace," in *Investment Casting*, P.R. Beeley and R.F. Smart, eds. (The Institute of Materials, London, 1995), p. 374.
2. A. Hellawell, J.R. Sarazin, and R.S. Steube, *Phil. Trans. R. Soc. Lond.* **345 A**: 507 (1993).
3. S.D. Felicelli, J.C. Heinrich, and D.R. Poirier, *Metall. Trans. B* **22B**: 847 (1991)
4. D.R. Poirier and J.C. Heinrich, "Simulations of Thermosolutal Convection in Directional Solidification," in *Model of Casting, Welding and Advanced Solidification Process VI*, T.S. Piwonka, V. Voller, and L. Katgerman, eds. (TMS, Warrendale, PA, 1993), pp. 227-234.
5. D.G. Neilson and F.P. Incropera, *Wärme-und Stoffübertragung* **27**; 1 (1992).
6. T. Fujii, D.R. Poirier, and M.C. Flemings, *Metall. Trans. B* **10B**: 331 (1979).
7. M.C. Schneider and C. Beckermann, *Metall. Mater. Trans. A* **26A**: 2373 (1995).
8. M.C. Schneider and C. Beckermann, *ISIJ In*. **35**: 665 (1995).
9. S.D. Felicelli, D.R. Poirier, and J.C. Heinrich, "Macrosegregation Patterns in Multicomponent Ni-base Alloys," *J. Cryst. Growth*, 1997, in press.
10. P.K. Sung, D.R. Poirier, and E. McBride "Estimating Densities of Liquid Transition-Metals and Ni-base Superalloys," *Mater. Sci. Eng. A*, in press (1977).
11. S.D. Felicelli, J.C. Heinrich, and D.R. Poirier, *Num. Heat Transfer* **23**: 461 (1993).
12. P. K. Sung, Ph.D. dissertation research in progress (The University of Arizona, Tucson, 1997).
13. P. Nash (Ed.), *Phase Diagrams of Binary Nickel Alloys* (ASM International, Materials Park, OH, 1991), p. 367.

14. G. Petzow and G. Effenberg (Eds.), *Ternary Alloys* (VCH, Weinheim, Germany, 1993), Vol. 8, p. 49.

15. S. N. Tewari, M. Vijayakumar, J. E. Lee, and P. A. Curreri, *Mater. Sci. and Eng. A* **141**: 97 (1991).

16. E. McBride and D. R. Poirier, Internal report to Investment Casting Cooperative Arrangement, contract no. MDA972-93-2-0001 (The University of Arizona, Tucson, 1996).

17. W. Betteridge and J. Heslop (Eds.), *The Nimonic Alloys and Other Nickel-Base High-Temperature Alloys* (Crane, Russak & Company, Inc., New York, 1974), 2nd ed., p. 161.

18. B. A. Mueller, Private communication (Howmet Research Center, Whitehall, MI, 1996).

19. D.R. Poirier, *Metall. Trans B* **18B**: 245 (1987).

14. G. Petzow and G. Effenberg (Eds.), *Ternary Alloys* (VCH, Weinheim, Germany, 1993), Vol. 8, p. 49.

15. S. N. Tewari, M. Vijayakumar, J. E. Lee, and P. A. Curreri, *Mater. Sci. and Eng. A* **141**: 97 (1991).

16. E. McBride and D. R. Poirier, Internal report to Investment Casting Cooperative Arrangement, contract no. MDA972-93-2-0001 (The University of Arizona, Tucson, 1996).

17. W. Betteridge and J. Heslop (Eds.), *The Nimonic Alloys and Other Nickel-Base High-Temperature Alloys* (Crane, Russak & Company, Inc., New York, 1974), 2nd ed., p. 161.

18. B. A. Mueller, Private communication (Howmet Research Center, Whitehall, MI, 1996).

19. D.R. Poirier, *Metall. Trans B* **18B**: 245 (1987).

Table 1. Thermodynamic and transport properties used in the simulations.

| Property | References |
|---|---|
| Reference Concentrations (wt. pct.): $c_R^{\mathrm{Al}} = 6,\ c_R^{\mathrm{Ta}} = 6,\ c_R^{\mathrm{W}} = 5$ | -- |
| Reference Temperature (K): $T_R = 1697$ | 12, 13 |
| Eutectic Temperature (K): $T_E = 1642$ | 14 |
| Equilibrium Partition Ratios: $k^{\mathrm{Al}} = 0.96$<br>$k^{\mathrm{Ta}} = 0.5655 + 0.0183\ c_l^{\mathrm{Ta}}$<br>$k^{\mathrm{W}} = 1.67$ | 12<br>12<br>15 |
| Liquidus Temperature (K):<br>$T_L = 1728 + 2.23354\ c_l^{\mathrm{Al}} - 0.0584719\ c_l^{\mathrm{Ta}} + 2.4\ c_l^{\mathrm{W}} - 2.45034(c_l^{\mathrm{Al}})^{1.5} - 0.384791(c_l^{Ta})^{1.5} - 0.96448(c_l^{\mathrm{Al}} c_l^{\mathrm{Ta}})^{0.75}$<br>[$c_k^{\mathrm{Al}}$, $c_l^{\mathrm{Ta}}$, and $c_l^{\mathrm{W}}$ in wt. pct.] | 12, 13 |
| Thermal Expansion Coefficient ($K^{-1}$): $\beta_T = -1.386 \times 10^{-4}$ | 10 |
| Solutal Expansion Coefficients (wt. pct. $^{-1}$):<br>$\beta_c^{Al} = -2.457 \times 10^{-2}$, $\beta_c^{Ta} = 4.617 \times 10^{-3}$, $\beta_c^{W} = 5.241 \times 10^{-3}$ | 10 |
| Viscosity (N s $m^{-2}$): $\mu = 4.635 \times 10^{-3}$ | 16 |
| Specific Heat (J $kg^{-1}$ $K^{-1}$): $c = 700$ | 17 |
| Latent Heat (J $kg^{-1}$): $L = 2.95 \times 10^5$ | 18 |
| Thermal Conductivity (W $K^{-1}$ $m^{-1}$): $\kappa = 30$ | 17 |
| Density (kg $m^{-3}$): $\rho_0 = 7194$ | 10 |
| Solute Diffusivity in Liquid ($m^2$ $s^{-1}$): $D = 5 \times 10^{-9}$ | -- |
| Primary Dendrite Arm Spacing ( μm): $d_1 = 400$ | -- |
| Permeability ($m^2$):<br>$K_x = \begin{cases} 1.09 \times 10^3 \phi^{3.32} d_1^2 & \phi < 0.65 \\ 4.04 \times 10^{-6} \left(\frac{\phi}{1-\phi}\right)^{6.7336} d_1^2 & 0.65 \le \phi < 0.75 \\ \left[-6.49 \times 10^{-2} + 5.43 \times 10^{-2} \left(\frac{\phi}{1-\phi}\right)^{0.25}\right] d_1^2 & 0.75 \le \phi < 1 \end{cases}$<br>$K_z = \begin{cases} 3.75 \times 10^4 \phi^2 d_1^2 & \phi < 0.65 \\ 2.05 \times 10^{-7} \left(\frac{\phi}{1-\phi}\right)^{10.739} d_1^2 & 0.65 \le \phi < 0.75 \\ 0.074\left[\log(1-\phi)^{-1} - 1.49 + 2(1-\phi) - 0.5(1-\phi)^2\right] d_1^2 & 0.75 \le \phi < 1 \end{cases}$ | 19 |

**FIGURE CAPTIONS**

Fig. 1. Rectangular domain showing initial and boundary conditions.

Fig. 2. Distribution of total concentration of W during solidification of Ni-6 Al-6 Ta-5 W (wt. pct.).

Time = 15 min.

a. Benchmark case

b. $k^{\mathrm{W}}$ decreased by 10%

c. $k^{\mathrm{W}}$ increased by 10%

d. $\beta_c^W$ decreased by 20%

e. $\beta_c^W$ increased by 20%

f. $\mu$ decreased by 25%

g. $\mu$ increased by 25%

Fig. 3. Distribution of total concentrations of Al during solidification of Ni-6 Al-6 Ta (wt pct.).

Time = 15 min.

Fig. 4. Solidification of Ni-6 Al-6 Ta-5 W (wt. pct.) for $r$ = 0.12 K/s and $k^{\mathrm{W}}$ increased by 10%.

Time = 8 min.

a. Total concentration of W

b. Velocity vectors and contour lines of fraction of liquid

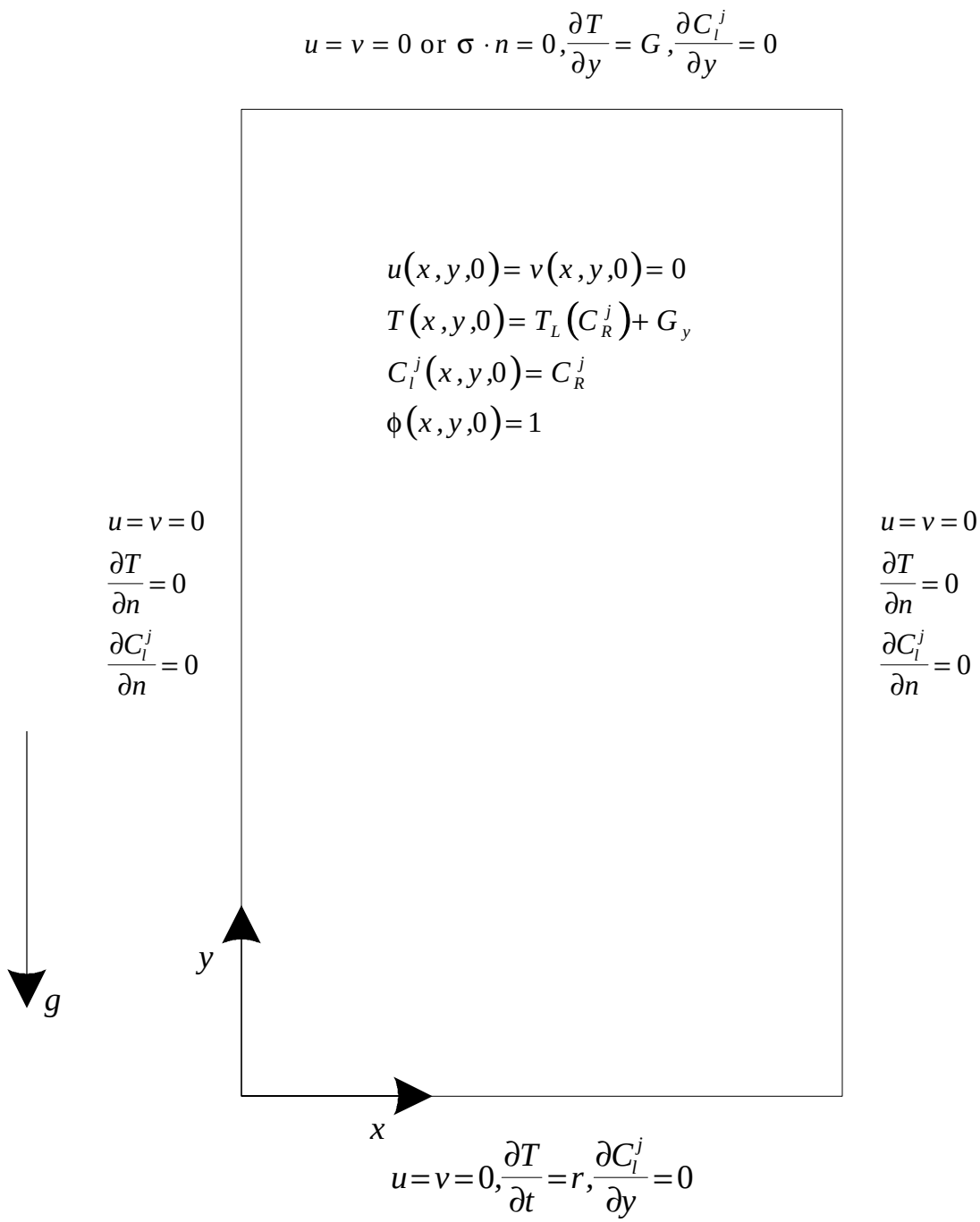
$u = v = 0$ or $\sigma \cdot n = 0, \frac{\partial T}{\partial y} = G, \frac{\partial C_l^j}{\partial y} = 0$
$u(x,y,0) = v(x,y,0) = 0$
$T(x,y,0) = T_L(C_R^j) + G_y$
$C_l^j(x,y,0) = C_R^j$
$\phi(x,y,0) = 1$
$u = v = 0$
$\frac{\partial T}{\partial n} = 0$
$\frac{\partial C_l^j}{\partial n} = 0$
$u = v = 0$
$\frac{\partial T}{\partial n} = 0$
$\frac{\partial C_l^j}{\partial n} = 0$
$g$
$y$
$x$
$u = v = 0, \frac{\partial T}{\partial t} = r, \frac{\partial C_l^j}{\partial y} = 0$

**Min = 4.43 , Max = 5.69**

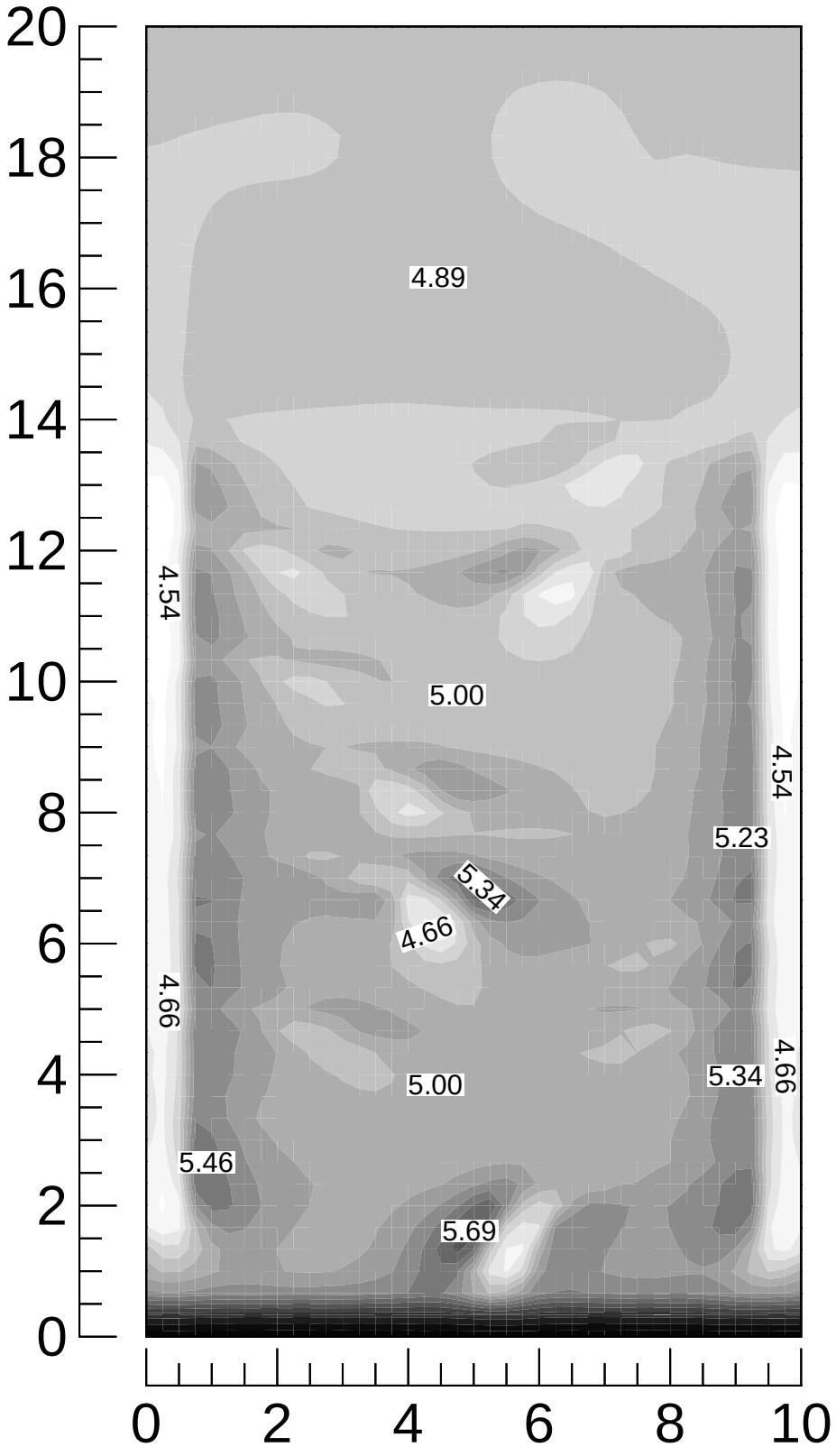

**Min = 4.61 , Max = 5.39**

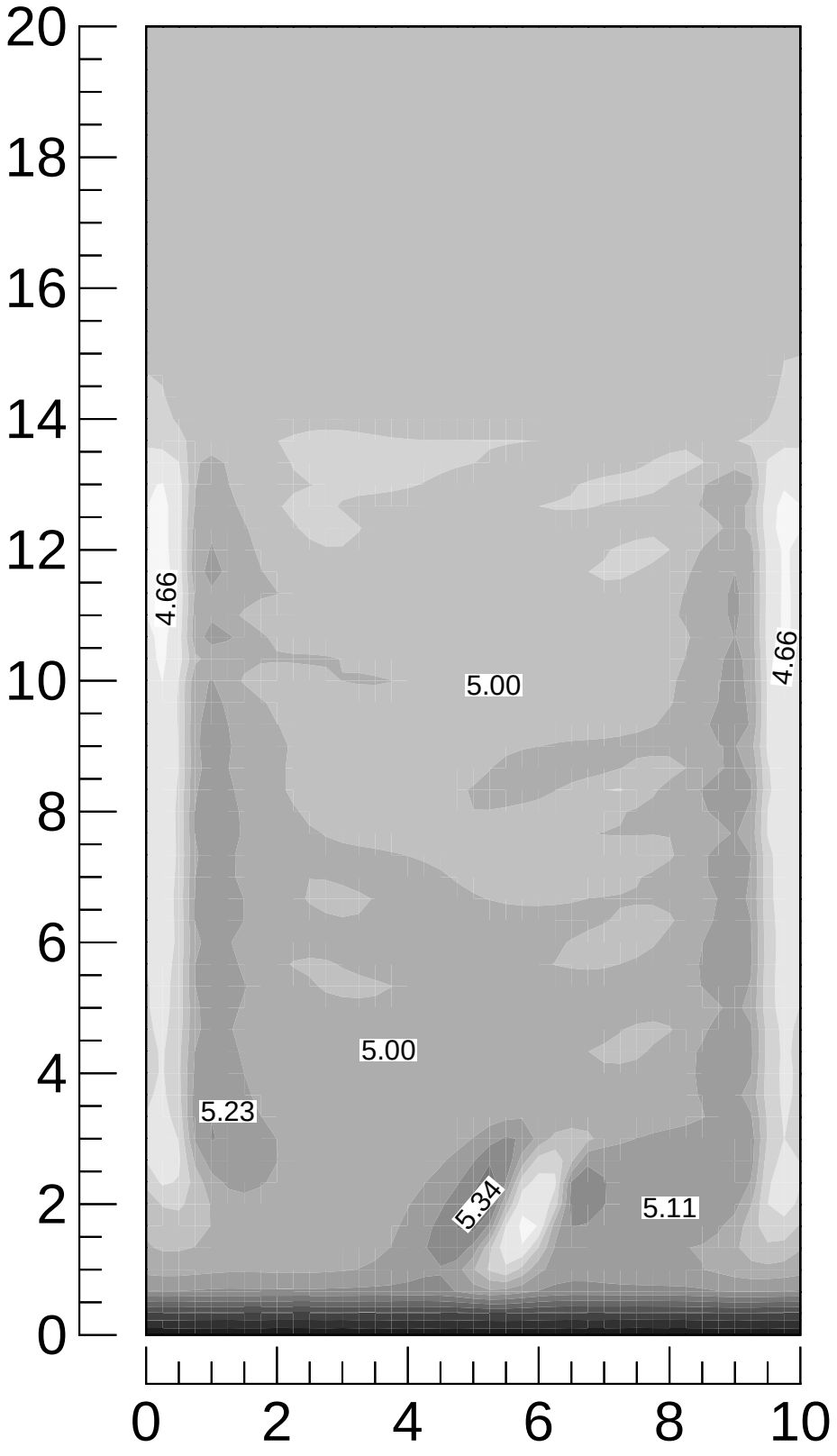

**Min = 4.24 , Max = 6.05**

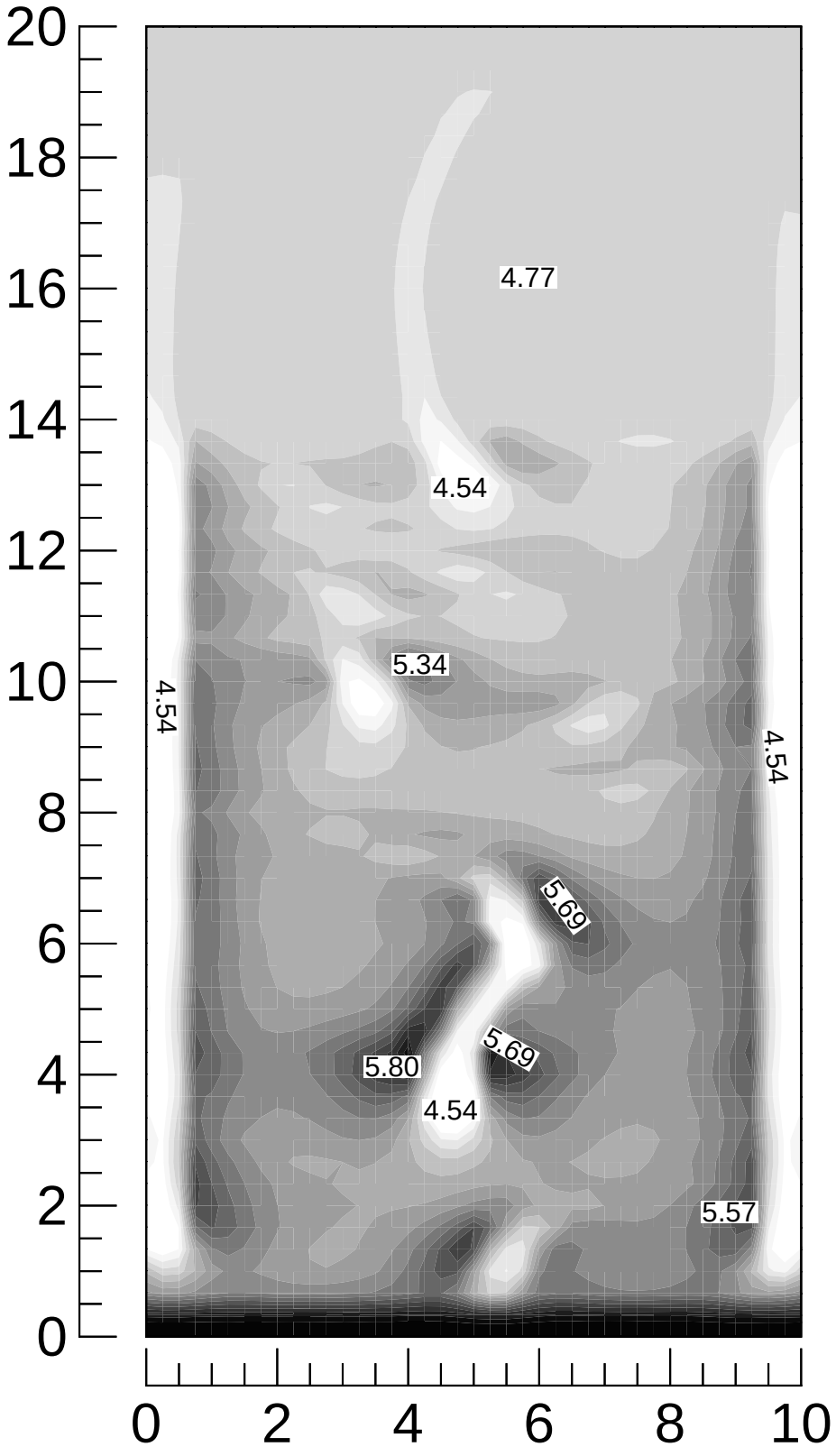

**Min = 4.49 , Max = 5.53**

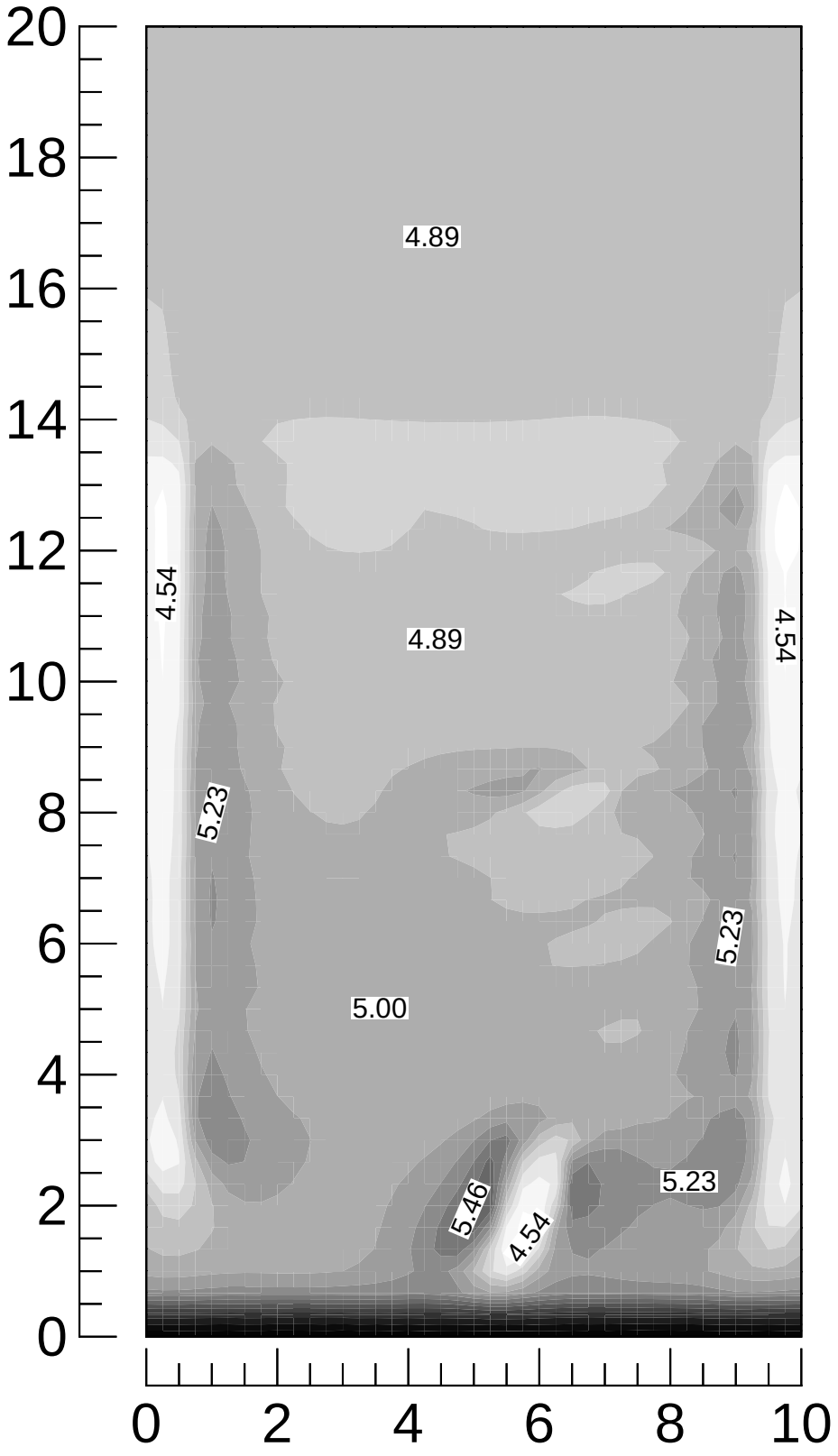

**Min = 4.38 , Max = 5.60**

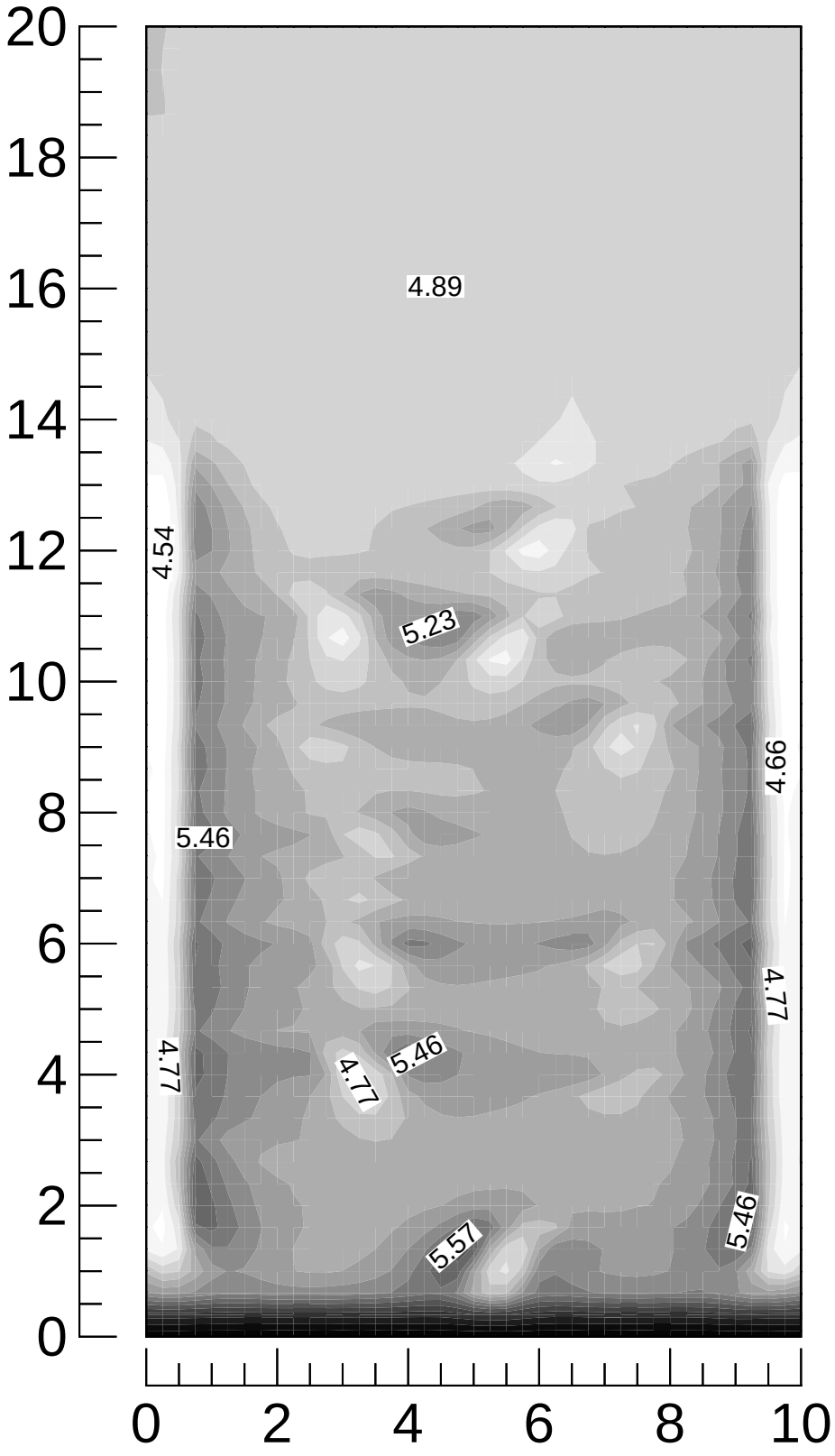

**Min = 4.36 , Max = 5.68**

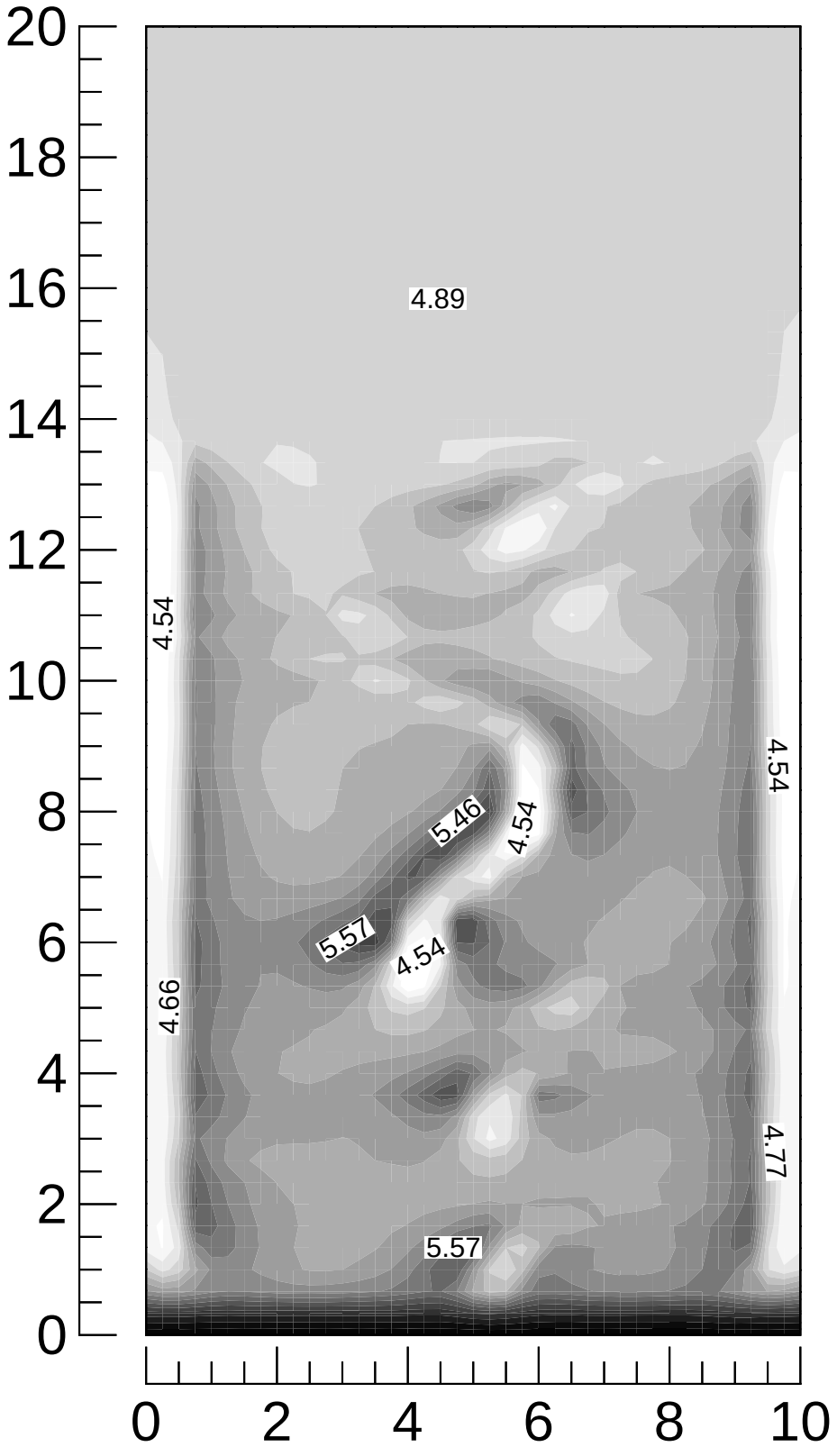

**Min = 4.48 , Max = 5.60**

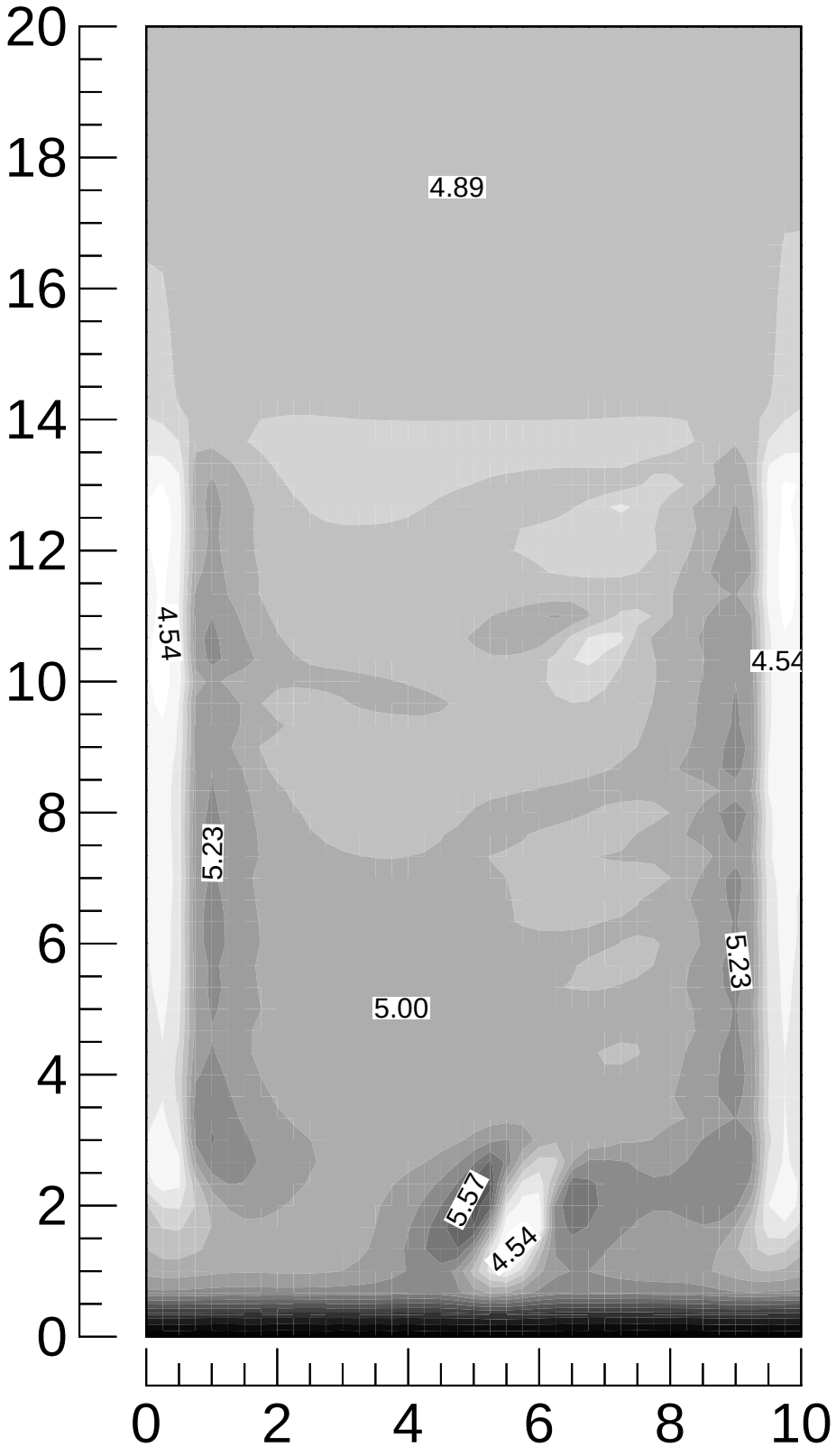

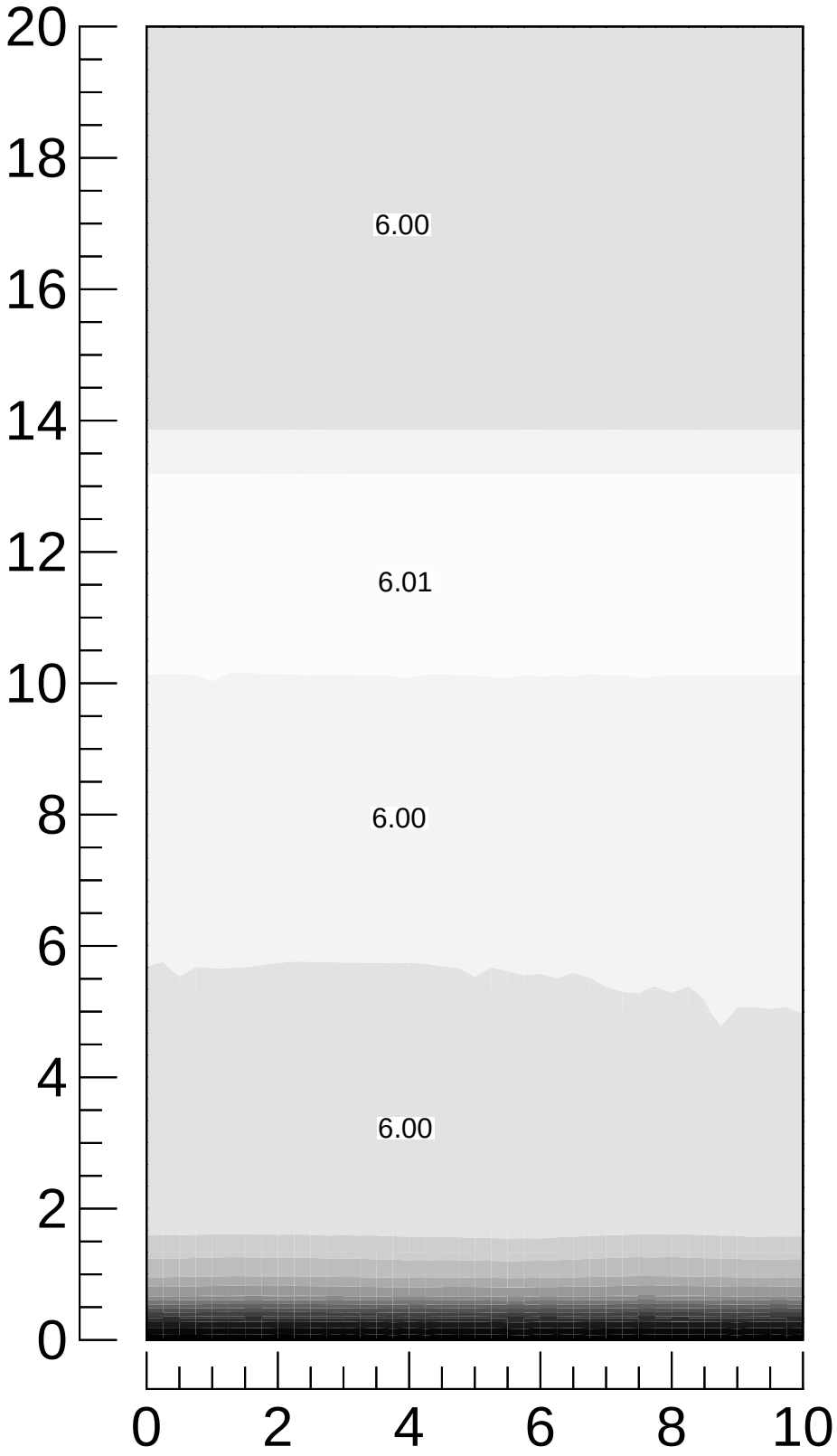
20
18
16
14
12
10
8
6
4
2
0
6.00
6.01
6.00
6.00
0
2
4
6
8
10

**Min = 4.20 , Max = 5.81**

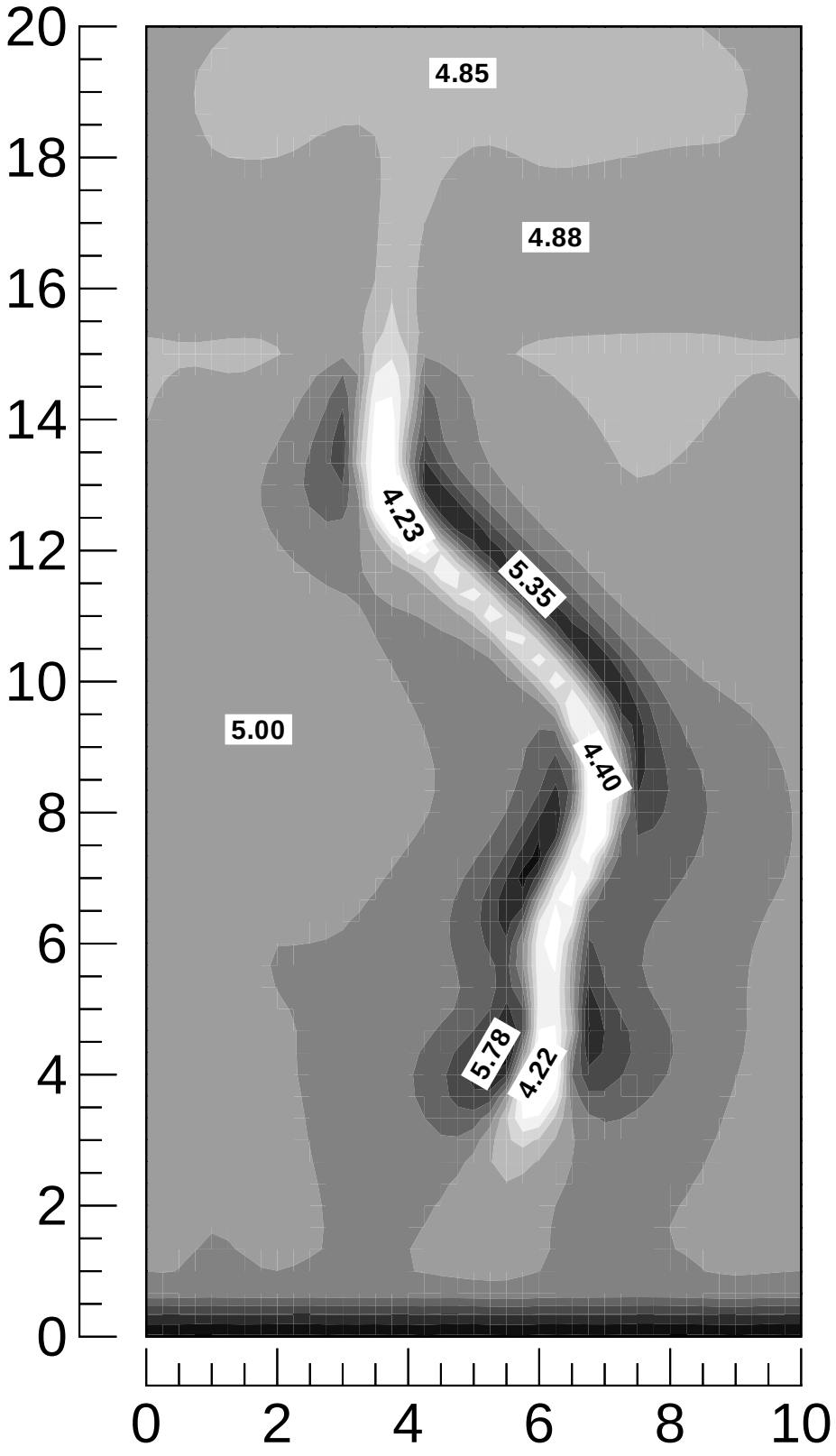

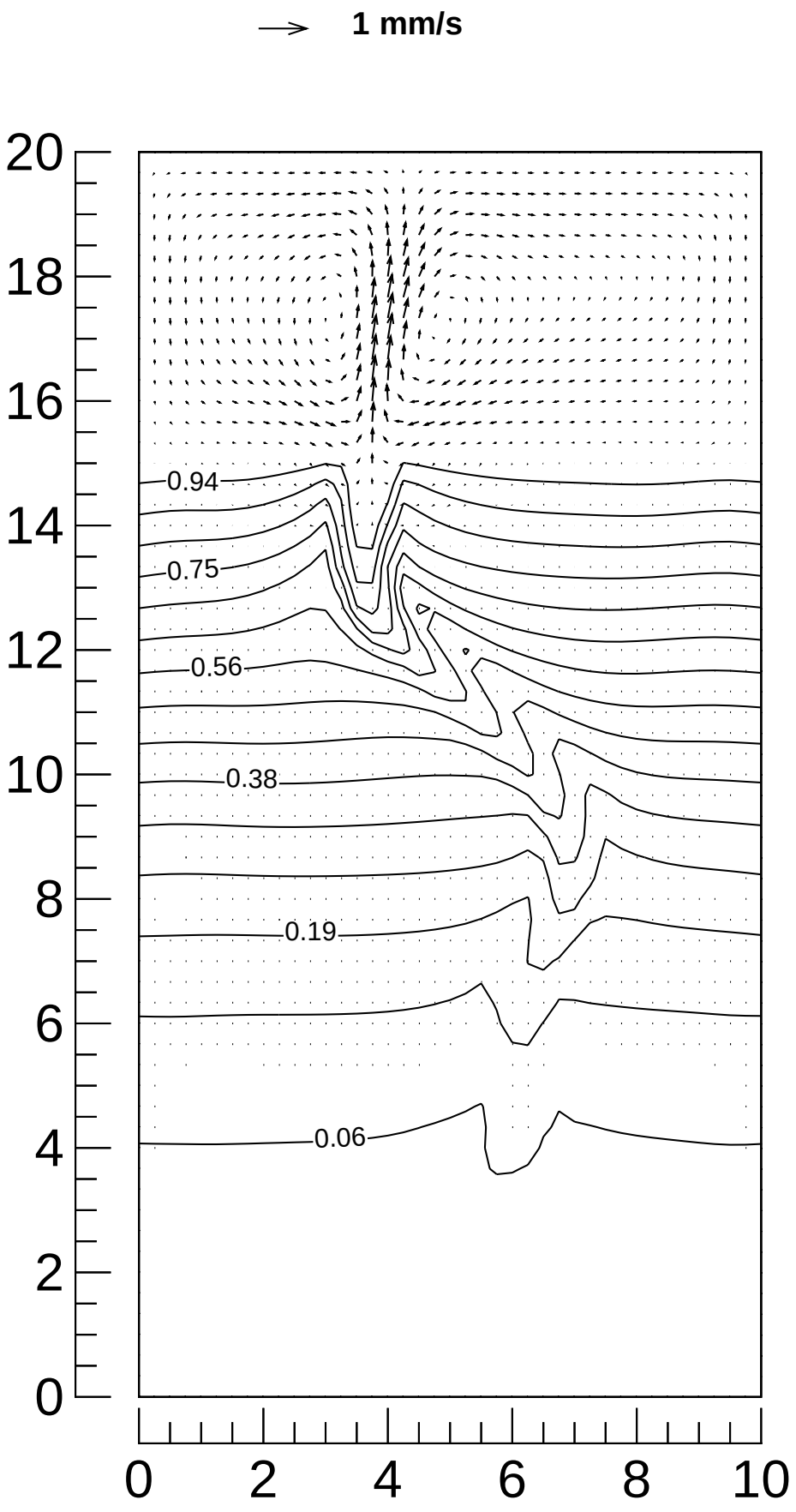
1 mm/s
0.94
0.75
0.56
0.38
0.19
0.06
0
2
4
6
8
10
12
14
16
18
20
0
2
4
6
8
10